AGU PUBLICATIONS

JGR

Journal of Geophysical Research: Atmospheres

RESEARCH ARTICLE
10.1002/2017JD026702

Key Points:
- High-resolution numerical simulations coupled with multilayer urban canopy model in the high-rise and highly compact city of Hong Kong
- Lower level convergence zone is due to combined effect of urban heat island circulation and sea-land breeze circulation
- A dome-shaped feature and wind stagnation phenomenon in the lower level convergence zone in the urban center in the Kowloon Peninsula

Supporting Information:
- Supporting Information S1

Correspondence to:
Y. Li,
liyg@hku.hk

Citation:
Wang, Y., S. Di Sabatino, A. Martilli, Y. Li, M. S. Wong, E. Gutiérrez, and P. W. Chan (2017), Impact of land surface heterogeneity on urban heat island circulation and sea-land breeze circulation in Hong Kong, *J. Geophys. Res. Atmos.*, *122*, 4332–4352, doi:10.1002/2017JD026702.

Received 28 FEB 2017
Accepted 4 APR 2017
Accepted article online 7 APR 2017
Published online 30 APR 2017

Impact of land surface heterogeneity on urban heat island circulation and sea-land breeze circulation in Hong Kong

Y. Wang[1,2], S. Di Sabatino[2], A. Martilli[3], Y. Li[1], M. S. Wong[4], E. Gutiérrez[5], and P. W. Chan[6]

[1]Department of Mechanical Engineering, University of Hong Kong, Hong Kong, [2]Department of Physics and Astronomy Alma Mater Studiorum, University of Bologna, Bologna, Italy, [3]Centro de Investigaciones Energéticas, Medioambientales y Tecnológicas, Madrid, Spain, [4]Department of Land Surveying and Geo-Informatics, Hong Kong Polytechnic University, Hong Kong, [5]Mechanical Engineering Department, City College of New York, New York, New York, USA, [6]Hong Kong Observatory, Hong Kong

Abstract Hong Kong is one of the most high-rise and highly compact cities in the world. The urban land surface is highly heterogeneous, which creates low-level convergence zones in urban areas, particularly the Kowloon Peninsula. The low-level convergence zone is due to the combined effect of urban heat island circulation (UHIC) and sea-land breeze circulation (SLBC) under weak northeasterly synoptic flow. To study the impacts of anthropogenic fluxes and built-up areas on the local circulation, the Weather Research and Forecasting (WRF) mesoscale model is combined with the multilayer urban canopy building effect parameterization/building energy model (BEP/BEM) parameterization to produce a 3 day simulation of an air pollution episode in Hong Kong in September 2012. To better represent the city land surface features, building information is assimilated in the central part of the Kowloon Peninsula. The WRF-BEP-BEM model captures the 2 m temperature distribution and local wind rotation reasonably well but overestimates the 10 m wind speed with a mean bias error of 0.70 m/s. A dome-shaped feature with a high level of moisture is captured in the convergence zones due to intensified UHIC and inflowing SLBC. The anthropogenic heat increases the air temperature by around 0.3°C up to 250 m, which in turn modifies the SLBC. A new drag coefficient based on λ_P, plan area per unit ground area, is tested. Besides the basic physical characteristics captured by the WRF-BEP-BEM model, the stagnation of wind in the lower level convergence zone is better captured by this approach than by the traditional constant value coefficient.

1. Introduction

Urban areas are already home to more than half of the world's population [*Wang et al.*, 2013; *Castles et al.*, 2013], and this percentage is continuously rising. Increased urbanization affects the environment within and above the urban canopy layers. For example, the presence of a city modifies the urban climate and local meteorology, which contributes to the formation of pollutant entrapment zones that reduce visibility and exacerbate morbidity [*Di Sabatino et al.*, 2010; *Arnfield*, 2003; *Rizwan et al.*, 2008, *Hunt et al.*, 2013].

This work focuses on the city of Hong Kong for several reasons.

1. For example, in the Kowloon Peninsula, it is one of the densest, high-rise, and compact cities in the world. Also, the maximum values of $\boldsymbol{\lambda_P}$, and $\boldsymbol{\lambda_B}$, building surface area per unit ground area, as defined by *Burian et al.* [2007], reaches 0.97 and 8.1, respectively, at a 250 m horizontal resolution. The mean building height is 55.2 m, the highest building in the area is around 130 m, and the standard deviation of the average building height is 32 m, which illustrates the horizontal and vertical heterogeneities of urban structures.
2. Studies have focused on the interactions of sea/land breeze circulations (SLBC) and urban heat island circulations (UHIC) in the Pearl River Delta region [*Tong et al.*, 2005; *Lo et al.*, 2006; *Wu et al.*, 2011]. However, the impact of land surface heterogeneity on the wind physics, especially around high-rise and highly compact buildings, the associated anthropogenic heat flux, and their effects on the interaction of UHIC and SLBC are still not clear. In addition, mesoscale models still need to accurately capture the diurnal wind speed and direction under a weak synoptic background, as the urban-land-surface model (LSM) model shows a positive wind speed bias for Hong Kong [*Lo et al.*, 2006].
3. The city is located in a transition zone of the East Asian monsoon system and receives large amounts of pollutants emitted in the East Asian Pacific Rim [*Chan and Chan*, 2000]. High air pollution events (especially elevated ozone) in Hong Kong are related to surface emissions, transport patterns, and meteorological conditions and occur mainly in autumn (September–November [*Chan et al.*, 1998]). The prevailing

wind direction in autumn is northeasterly. On 15–18 September 2012, a record high air pollution episode occurred in Hong Kong. The synoptic conditions, with a northeasterly prevailing wind, were favorable for creating a severe pollution episode, as described in section 2.5.

4. Sufficient surface, radiosonde, and wind profile observational data provided by the Hong Kong Observatory and air quality monitoring data from the Environmental Protection Department (EPD) are available.
5. Due to the peculiar urban structure and the complex topography, it is challenging for mesoscale models to capture the horizontal and vertical extensions of sea breezes and urban forcing. In this context, a correct representation of the city is crucial. The parameterizations in state-of-the-art mesoscale models are single-layer urban canopy models (UCM) [e.g., *Liu et al.*, 2006; *Johnson et al.*, 1991; *Grimmond and Oke*, 1999; *Masson*, 2000; *Kusaka et al.*, 2001; *Oleson et al.*, 2008; *Silva et al.*, 2009; *Wang et al.*, 2013] and multilayer UCMs [*Martilli*, 2002; *Kondo et al.*, 2005]. A multilayer scheme is considered the most appropriate for representing cities such as Hong Kong, with very high buildings and high variability. The building effect parameterization (BEP) scheme [*Martilli et al.*, 2002] was thus chosen for this study. This scheme was coupled with a simple building energy model (BEM) [*Salamanca and Martilli*, 2010] that estimates the anthropogenic heat flux from buildings by computing the energy budget for the building interior, accounting for energy generation by occupants and equipment, heat diffusion through walls, ventilation, and radiation through the windows. The scheme has already been tested on several cities (New York [*Gutiérrez et al.*, 2015a], Athens [*Martilli et al.*, 2003], Houston [*Salamanca et al.*, 2011], and Madrid [*Salamanca et al.*, 2012]). Comparisons of the scheme's performance with measurements, single urban canopy layer parameterizations, and traditional schemes based on Monin-Obukhov similarity theory show that it is able to reproduce the vertical structure of urban roughness, vertical potential temperature profiles, and near-surface wind and temperature patterns.

The research questions that motivate this work are as follows.

1. Can a mesoscale model represent a high-rise and highly compact city like Hong Kong? In particular, are the drag forcing, turbulence, and thermal fields well reproduced within an urban canopy characterized by a nonuniform building height distribution?
2. How do the UHIC, SLBC, and surface heterogeneity interact under the weak synoptic background for Hong Kong?

The rest of this paper is organized as follows: section 2 provides a description of urban canopy parameters and the implementation of a new drag coefficient, an overview of the study area, the meteorological conditions on the selected days, and a description of the coupled Weather research Research and forecasting Forecasting (WRF)-BEP-BEM modeling system; section 3 presents an evaluation and analysis of the WRF-BEP-BEM model results compared with the observational data; section 4 provides a further discussion of the factors that influence the development of sea breezes and UHIC; and section 5 presents a summary and conclusions.

2. Data and Methodology

2.1. Study Area

The high-rise, dense, and well-developed city of Hong Kong (22°N, 114°E) is located on the southeastern coast of China, within the Asian continent. Hong Kong's climate is dominated by Asian continental high pressure during autumn and winter and mainly by low pressure in summer [*Chan et al.*, 1998]. The prevailing wind direction is northeasterly in winter and southwesterly in summer, which causes two completely different air masses to reach the urban areas of Hong Kong. The climate is influenced by subtropical and Asian monsoonal conditions with cool and humid winters, and hot and wet summers. The Pearl River Delta region, which includes the province of Guangdong and the Hong Kong Special Administrative Region, is one of the fastest-growing areas in the world, with rapidly developing industrialization and urbanization [*Chan and Chan*, 2000]. The nearest city in mainland China, Shenzhen, a special economic zone, is roughly 35 km north of the urban center of Hong Kong [*Chan et al.*, 1998]. The total area of Hong Kong is about 1000 km^2, but the topography is extremely rugged with 75% hilly areas (the highest point of Hong Kong is 957 m at Tai Mo Shan), little naturally flat land, and a complex coastline [*Tong et al.*, 2005]. In mid-2014, the population of Hong Kong was 7.24 million (http://www.gov.hk/), 95% of whom lived and worked in less than 20% of the

Figure 1. Schematic representation of gridded building assimilation in urban areas. (a) Photo of the area. (b) Detailed building information (30 m resolution). (c) Urban morphology in each grid point at a 250 m resolution; A_P is the plan area, A_W is the building wall area, and A_T is the total surface area. (d) Two-dimensional assimilation in the BEP model; w is the width of the street, b is the width of the buildings, and h_i is the building height; each floor is assumed to be 5 m in height; (bottom) our simplified BEP model: $\acute{H}$ is the average weighted mean building height and σ is the standard deviation.

land area (http://www.pland.gov.hk/), mainly concentrated in the Kowloon Peninsula and the northern edge of Hong Kong Island on the two sides of Victoria Harbor.

2.2. Urban Morphological and Aerodynamic Parameters in Mesoscale Modeling

The Kowloon Peninsula (latitude from 22.2932°N to 22.3406°N and longitude from 114.1489°E to 114.2024°E), with available detailed three-dimensional building information in the innermost domain, is shown in Figures 1a and 1b. Note that the urban parameters for other areas in the innermost domain are set by default. The street orientations are set to 15° and 75°, respectively. To reduce the computational cost, buildings are grouped into three representative types with a height of $\acute{H}-\sigma$, $\acute{H}$, and $\acute{H}+\sigma$ for each grid. The average weighted mean building height, $\acute{H}$, and standard deviation, σ, are computed for every grid point following *Di Sabatino et al.* [2010]:

$$\acute{H} = \frac{\sum_{i=1}^{N} A_{pi} h_i}{\sum_{i=1}^{N} A_{pi}} \tag{1}$$

$$\sigma = \sqrt{\frac{1}{N-1}\sum_{i=1}^{N}\left(h_i - \acute{H}\right)^2} \tag{2}$$

where A_{pi} is the plan area of building i, h_i is the corresponding building height, and N is the number of buildings in the grid cell.

The other urban canopy parameters needed by the BEP-BEM, the plan area per unit ground area and building surface area per unit ground area, are also computed for every grid point. Then, nearest neighbor interpolation is used in agreement with the 0.5 km resolution for the innermost domain shown in Figures 2a and 2b.

The dominant sink of momentum in the urban canopy is the drag induced by the vertical surfaces of the buildings, which is parameterized following *Martilli et al.* [2002].

$$\acute{F}u_{IU}^{V} = -\rho C_{\text{drag}} \left| U_{IU}^{\text{ort}} \right| \overrightarrow{U}_{IU}^{\text{ort}} S_{IU}^{V} \tag{3}$$

where $\overrightarrow{U}_{IU}^{\text{ort}}$ is the wind speed orthogonal to the street canyon direction at the IU level and S_{IU}^{V} represents the total wall surfaces at the IU level [*Martilli et al.*, 2002]. In the original BEP model, the drag coefficient C_{drag} is set to a constant value of 0.4. This constant value is taken from the wind tunnel experiment by *Raupach* [1992] and is widely used in modeling [*Uno et al.*, 1989]. However, this constant value could be a limitation when estimating the momentum flux or aerodynamic parameters in urban canopy layers. *Miao et al.* [2009] improved the drag coefficient term by using the formula from *Coceal and Belcher* [2005]. *Santiago et al.* [2008] found that the drag coefficient could vary with the building packing density based on the computational fluid dynamic results. *Santiago and Martilli* [2010] provided a new implementation with an array of cubes of the same height ($h/W = 1$, where h and W are the height and width of each cube, respectively). Thus, the drag coefficient becomes a function of the plan area per unit ground area, λ_P. The new

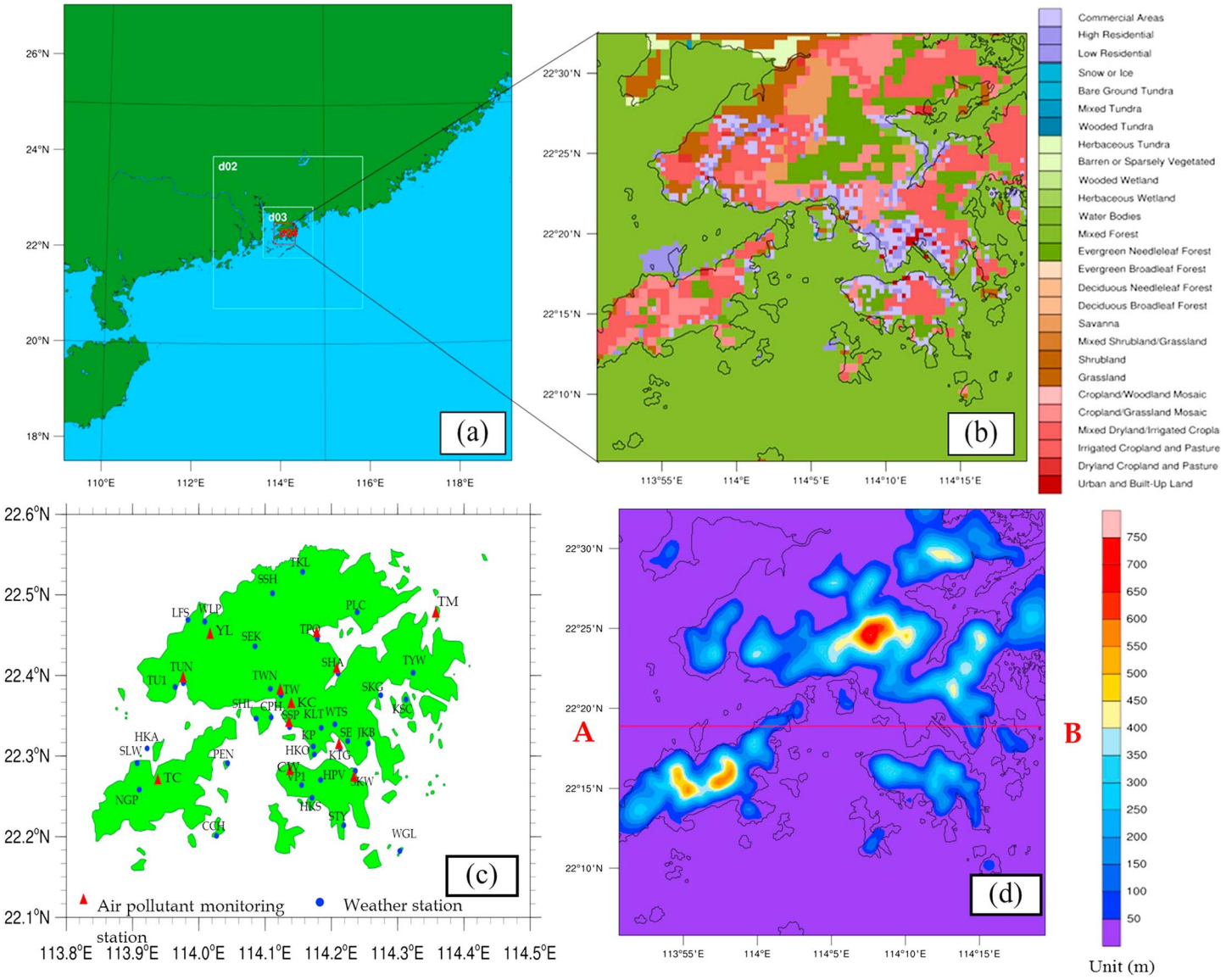

Figure 2. (a) WRF modeling domain with horizontal grid spacing of 13.5, 4.5, 1.5, and 0.5 km for domains d01, d02, d03, and d04, respectively. (b) Modified LCLU data for the innermost domain with three urban classes (the light purple refers to class 1, the moderate purple refers to class 2, and the dark purple refers to class 3). (c) Location of observation stations: the red triangles show the locations of air pollution monitoring stations, and the solid blue circles indicate weather stations. (d) Terrain height for the innermost domain, with the transect A–B indicating the location of the spatially filtered cross-sectional indicators discussed in section 4.

implementation of the drag coefficient term in equation (3), which is discussed in section 4, is as follows [*Santiago and Martilli*, 2010; *Gutiérrez et al.*, 2015b]:

$$C_{\mathrm{drag}_{\mathrm{new}}} = \begin{cases} 3.32\lambda_P{}^{0.47}, \text{ when } \lambda_P \le 0.29 \\ 1.85, \text{ when } \lambda_P > 0.29 \end{cases} \tag{4}$$

where λ_P is the plan area per unit ground area.

2.3. Modified Urban Land Cover and Land Use Data

Land cover and land use (LCLU) data are important for accurately simulating urban effects [*Holt and Pullen*, 2007], especially in high-rise and compact cities. In accordance with the BEP-BEM urban classifications, which constrain urban land use to three categories, the latest (2012) 0.5 km spatial resolution LCLU data were used. The LCLU data were further classified as class 1 (industrial estates, airports, and public utilities), class 2 (private

and public residential buildings), and class 3 (commercial offices and government facilities), as shown in Figure 2b. Some of the parameters for the three urban classes used in the WRF-BEP-BEM model are provided in Table S1 in the supporting information. For the regions outside the Hong Kong area, U.S. Geological Survey 24-category LCLU data were used.

2.4. Modeling Systems and Configuration

The WRF model is a nonhydrostatic, compressible model with a mass coordinate system [*Skamarock et al.*, 2008]. The advanced research configuration of the WRF, version 3.6.1, was used to study a 3 day (72 h) simulation for 15–18 September 2012. The first day (15 September) was considered as spin-up time for this study. Four two-way nested domains were built with 79×79, 79×79, 79×79, and 100×100 grid points with spatial resolutions of 13.5, 4.5, 1.5, and 0.5 km, respectively (Figure 2a). The fourth domain covers Hong Kong's urban areas and the surrounding suburban and rural areas (Figure 2b). The vertical grid contains 51 terrains following full sigma levels from the ground up to 50 hPa. The planetary boundary layer (PBL) scheme of *Bougeault and Lacarrere* [1989] was used to predict the turbulent kinetic energy (TKE) and diffusion coefficients. The other physical schemes used in this study were the single-moment three-class microphysics scheme [*Hong et al.*, 2004], Dudhia shortwave radiation [*Dudhia*, 1989], rapid radiative transfer model longwave radiation [*Mlawer et al.*, 1997], and Noah land surface model [*Chen and Dudhia*, 2001], and the *Kain and Fritsch* [1990] cumulus schemes that were used for the outer two domains. The initial and boundary conditions for the WRF model were taken from the National Centers for Environmental Prediction Global Forecast System Final Analyses data (FNL) at 1° at 6 h intervals. Daily sea surface temperatures from National Centers for Environmental Prediction Marine Modeling and Analysis Branch data at 0.5° were used.

The BEP-BEM multiple-layer urban canopy model developed by *Martilli* [2002] was coupled with WRF model 3.6.1 to represent the dynamics and thermal effects of urban areas. The BEP considers (1) 2-D street canyons with two different orientations (15° and 75° in this study), comprising an array of buildings of the same width and same distance from each other but with different building heights; (2) heat fluxes in ground surfaces and horizontal and vertical building surfaces due to radiation shadowing effects; (3) building drag effects with consequent loss of momentum; and (4) transformation of the mean-motion kinetic energy into TKE. The BEM [*Salamanca and Martilli*, 2010] was developed to calculate the amount of heat that must be released or added to each vertical building layer to maintain the target indoor air environment. The mesoscale model provides the BEM with the outdoor air temperature, air humidity, and boundary conditions for calculating the temperature of building walls and roofs. In turn, the BEM provides the heat fluxes and energy consumption of the buildings, taking the occupants and equipment into account [*Salamanca et al.*, 2014].

2.5. General Meteorological Conditions for the Case Study

On 15–18 September 2012, a record high air pollution episode occurred in Hong Kong. On 17 September, the ozone concentration at the Tung Chung, Shatin, and Shan Shui Po monitoring stations was over 100 ppb and the air pollution index (which was used by the Hong Kong EPD from June 1995 to December 2013) exceeded 100 at several stations, indicating very high levels of air pollution. The weather in Hong Kong that month was drier than usual due to the lack of tropical cyclones and the prevalence of continental air masses for part of the month (http://www.hko.gov.hk). Between 15 and 18 September, a typical cold front associated with a severe air pollution episode occurred in Hong Kong. Observational data (not shown here) indicate that before the arrival of the cold front, an anticyclone dominated over southern China with a prevailing southeasterly wind. As the cold front was approaching, the northeast monsoon behind the front made the weather dry and cooler (http://www.hko.gov.hk). During the entire period, low-level winds over the Hong Kong area remained weak (2–5 m/s at ground level at Waglan Island from the observational data; 5–10 m/s at 850 hPa, as shown in Figure 3). The period was characterized by calm and cloudless weather, no precipitation, around 11 h of sunshine, and light winds—conditions that were favorable for the development of a UHI [*Chen et al.*, 2014] and sea-land breezes [*Zhang and Zhang*, 1997].

2.6. Numerical Experiments

The criteria chosen for the numerical experiments are summarized in Table 1. A control experiment was carried out to investigate and evaluate the model performance (hereafter referred to as the WRF-BEP-BEM and regarded as the Baseline Case), using new LCLU data, new urban canopy parameters, the coupled BEP/BEM model in urban areas, and a constant drag coefficient. Three sensitivity tests were carried out as

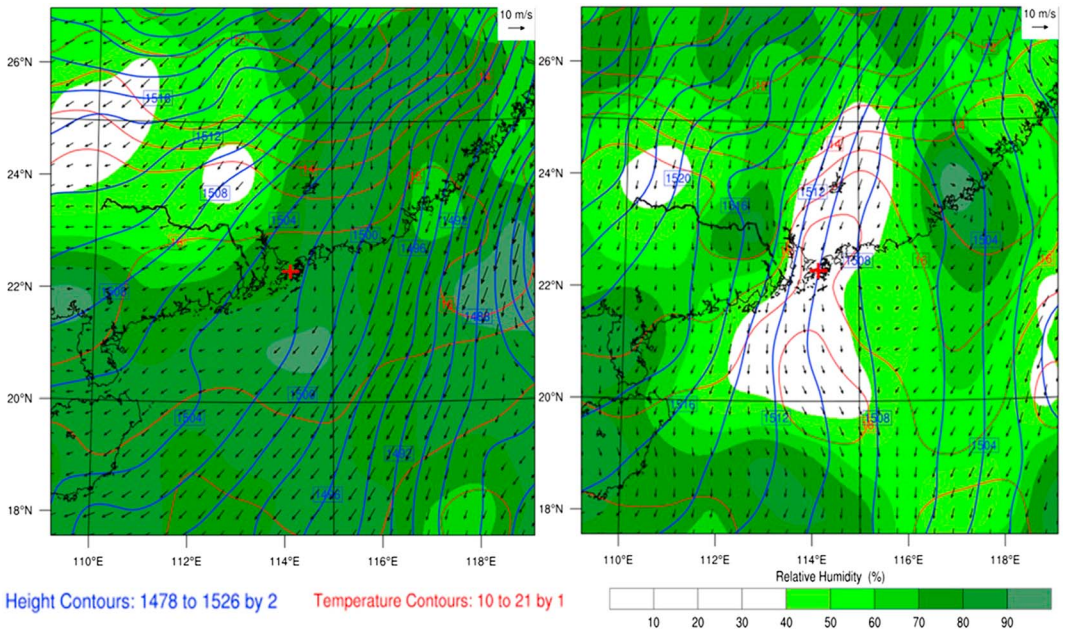

Figure 3. Synoptic weather patterns at 00:00 UTC (8:00 am local time) on 16 (left) and 17 (right) September 2012; the FNL reanalysis data provided the geopotential height (solid lines in blue), temperature (solid lines in red), wind speed and direction (arrows), and relative humidity (shaded) at 850 hPa. The red cross indicates the location of Hong Kong.

follows: (1) urban areas were replaced by grassland in the innermost domain to investigate the effect of urban areas on the local circulation, (2) anthropogenic heat was excluded,; and (3) the drag coefficient was chosen as the function mentioned in section 2.2.

3. WRF-BEP-BEM Simulation Evaluation

The control experiment (Baseline Case) starts at 00:00 UTC (08:00 A.M. local time) on 15 September 2012 and ends at 00:00 UTC 18 September 2012. To validate the control experiment with the WRF-BEP-BEM model, the simulation results are compared with observational data obtained from the Hong Kong Observatory. There are 36 surface meteorology stations available for this study (indicated by the blue solid circles in Figure 2c). Due to the highest horizontal spatial resolution of 0.5 km in the innermost domain, 28 meteorology stations are chosen for comparison, 16 of which are located in urban areas according to the modified LCLU data, as shown in Figure 2b. The stations at 0.5 km resolution scale that contain both land and sea surfaces are excluded as they may represent the sea surface characteristics [*Tong et al.*, 2005]. The observed variables are 10 m wind speed and wind direction averaged over 10 min, 2 m air temperature, and relative humidity.

3.1. Diurnal Wind Rotation

The sea breeze is a meteorological phenomenon that has been extensively studied by theoretical and numerical methods in many coastal areas [*Chen et al.*, 2009; *Li et al.*, 2016; *Tong et al.*, 2005]. Because of Hong Kong's complex urban environment and topography, it is still crucial to accurately capture the onset and propagation of sea breeze fronts. Moreover, several convergence zones are formed when a sea breeze propagates into inland areas, as described below. Numerical sea-land breeze models are critical for forecasting air quality in future studies.

Hong Kong's urban areas are located along the coastline, as shown in Figure 2b. Hence, it is important to verify whether the WRF-BEP-BEM simulation accurately captures the sea-land breeze as it is a potential source of fresh air. The diurnal evolution of observed and simulated surface wind at a height of 10 m on 17 September is shown in Figure 4. The Waglan Island (WGL) station can indicate the wind rotation because it is on an isolated island unaffected by urban heterogeneity. The WRF-BEP-BEM model captures well the diurnal wind rotation at this station, although it underestimates the wind speed during the day. One possible explanation is the limited resolution in the model [*Salamanca et al.*, 2011; *Tong et al.*, 2005]. On 17 September, the wind

Table 1. Indicators Used in Each Numerical Experiment

Numerical Simulations	Urban Scheme	Gridded Building Information	Anthropogenic Heat	Drag Coefficient
Baseline Case: WRF-BEP-BEM	BEP/BEM	Yes	Yes	$C_{drag} = 0.4$
Green Case: urban area modeled as grassland	No	No	No	$C_{drag} = 0$
No-heat Case: urban area modeled without any anthropogenic heat	BEP/BEM	Yes	No	$C_{drag} = 0.4$
New-drag Case: urban area with improved drag coefficient calculation	BEP/BEM	Yes	Yes	$C_{drag} = C_{drag_{new}}$

direction at the WGL station is northeasterly in the morning, then gradually changes to southeasterly in the afternoon with a reduction in wind speed, and gradually back to northeasterly during the night. The WRF-BEP-BEM model reasonably well captures the diurnal wind rotation in the stations along the coastline and the onset of the sea breeze at around 04:00 to 06:00 UTC (12:00 to 14:00 local time) at the Hong Kong Observatory station on the Kowloon Peninsula, the Wong Chuk Hang station in Hong Kong Island, and the Hong Kong International Airport, and Sha Lo Wan (SLW) stations near Hong Kong International Airport.

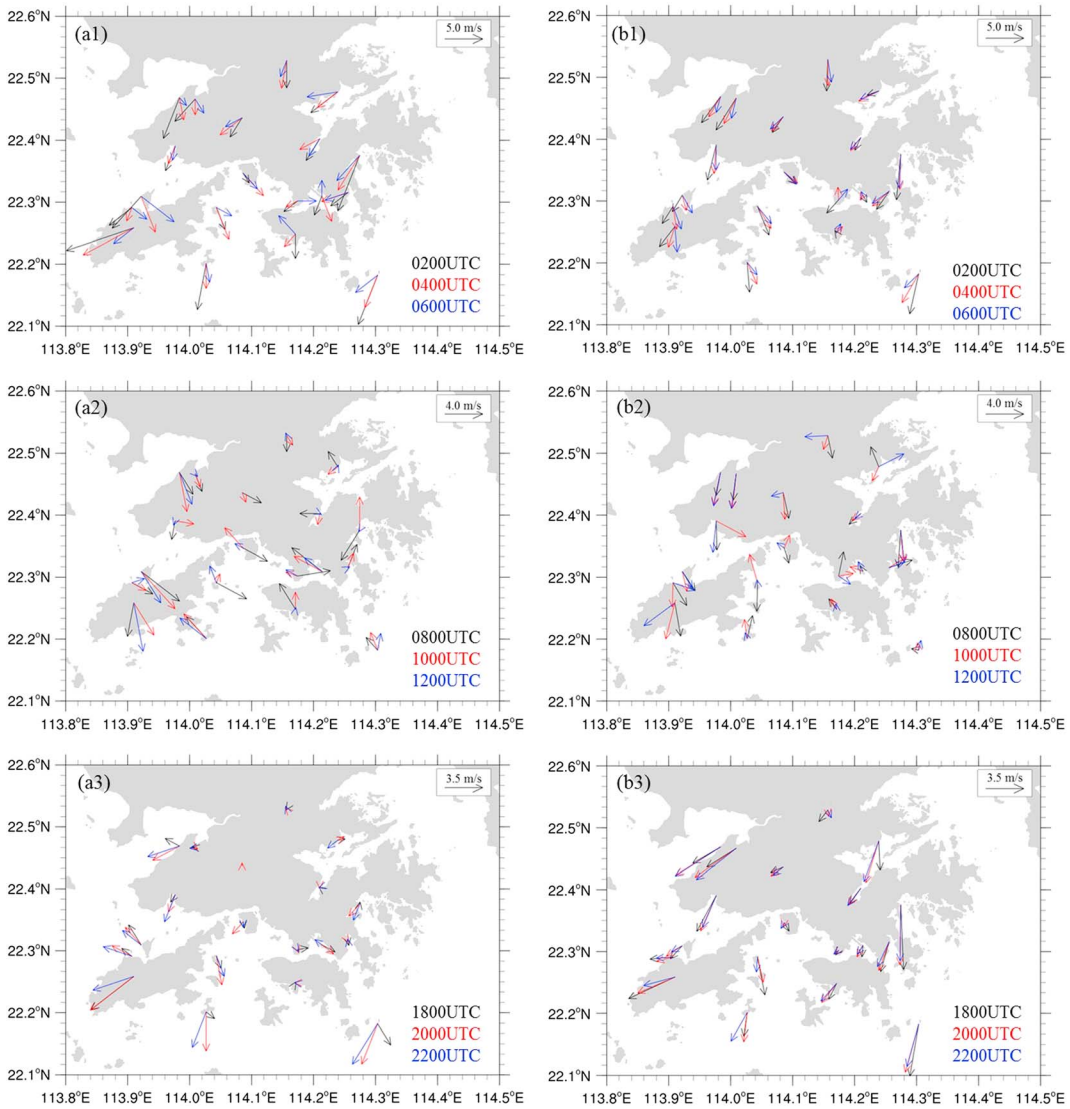

Figure 4. Diurnal evolution of 10 m wind speed and wind direction at 19 meteorological stations in Hong Kong on 17 September 2012. All times are UTC; for local time add 8 h. Observational data (a1) 02:00, 04:00, and 06:00; (a2) 08:00, 10:00, and 12:00; and (a3) 18:00, 20:00, and 22:00. Simulation results from case 1 (Baseline) (b1) 02:00, 04:00, and 06:00; (b2) 08:00, 10:00, and 12:00; and (b3) 18:00, 20:00, and 22:00.

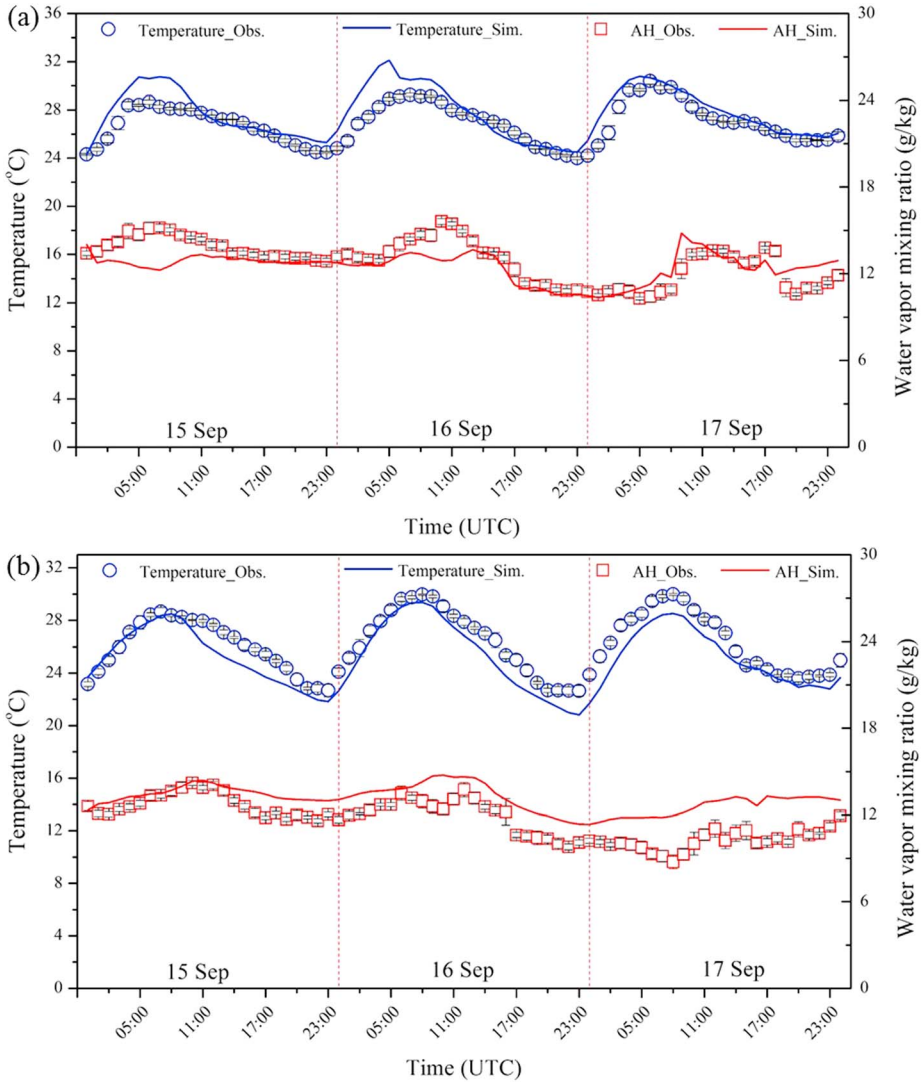

Figure 5. Predicted and measured 2 m air temperature and water vapor mixing ratio at two weather stations: (a) HKO and (b) LFS. The vertical bars represent the standard deviation of the 2 m air temperature.

The model captures the multiple sea breezes in different parts of Hong Kong well. However, the model does not adequately capture the offshore land breeze in the evening from 10:00 to 12:00 UTC (18:00 to 20:00 local time) on 17 September at the Hong Kong Observatory (HKO) station, which is located in the commercial area on the Kowloon Peninsula. This station is located in the convergence zone where the sea breeze penetrates inland, and it is difficult to recognize the wind direction at a spatial resolution of 0.5 km, which is discussed in section 4.

3.2. Spatial Distribution of Near-Surface Variables

Two individual stations, HKO and Lau Fau Shan (LFS), which are considered as urban and rural stations, respectively, according to the modified LCLU data mentioned in section 2.3, are chosen for the verification of 2 m air temperature and 2 m water vapor mixing ratio. HKO is located in a commercial area on the Kowloon Peninsula and is considered to be an urban station for many studies of the UHI phenomena in Hong Kong [*Siu and Hart*, 2013]. LFS is located on the shore of Deep Bay in the New Territories, which is less affected by the urban effect. Figure 5 shows that the model simulation results and observational data are in good agreement at both stations. On 16 and 17 September, the model underestimates the air temperature and overestimates the water vapor mixing ratio at the LFS station, perhaps because this station is located very close to the sea. A possible explanation is the 0.5 km spatial resolution, which may cover both sea and land in

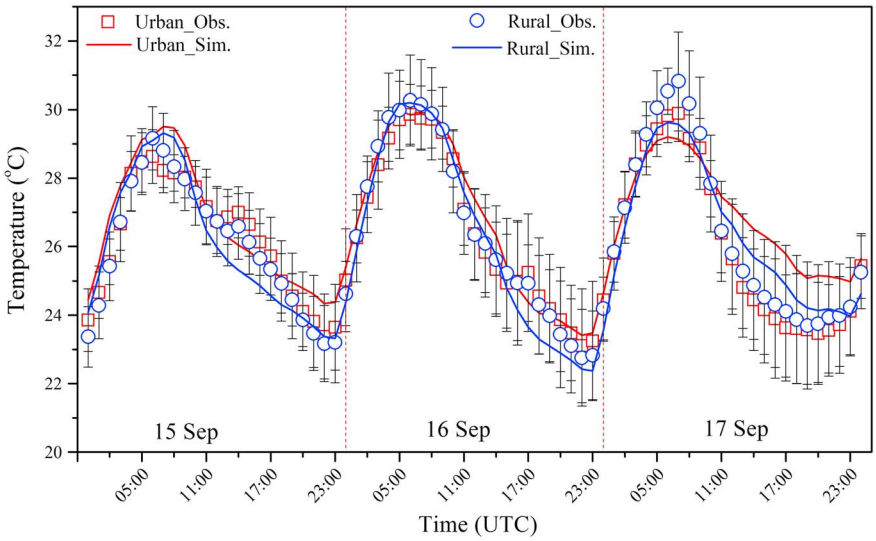

Figure 6. Comparison of observed and simulated 2 m air temperature (°C) for all urban and rural sites from 00:00 UTC on 15 September 2012 to 00:00 UTC on 18 September 2012 for domain 4. The vertical bars represent the standard deviation of the 2 m air temperature.

that grid point. On 17 September, the model captures the air temperature and water vapor mixing ratio at the HKO station, suggesting that individual stations may have local factors that lead to discrepancies.

Figure 6 compares the observed and simulated 2 m air temperature for 3 days for all urban and rural sites to avoid the influences from individual stations. Note that because the horizontal spatial resolution is limited to 0.5 km, the stations along the coast (Cheung Chau, Tseung Kwan O, Kau Sai Chau, WGL, Peng Chau, Wetland Park, SLW, and Tsak Yue Wu, as shown in Figure 2c) are excluded because they may represent sea surface characteristics. The WRF-BEP-BEM model (Baseline Case) captures the heterogeneous distribution of air temperature in both urban and rural areas. The model also captures the UCI phenomenon in urban areas during the day, which, although less studied, was confirmed by *Yang et al.* [2016] using a lumped air temperature model. The use of multilayer urban canopy parameterization can significantly improve the prediction of air temperature in comparison to a WRF simulation by using Noah LSM [*Chen and Dudhia*, 2001] without the UCMs (not shown here), which shows the air temperature as 2 °C lower in the urban areas. In this case, the temperature difference between the sea surface and urban areas is not sufficient for a sea breeze to develop, as explained in section 4. The WRF-BEP-BEM model captures the daytime UCI on 17 September, although it underestimates the air temperature in the rural and urban areas. One possible explanation is that there are some rural sites along the coastline and the sea surface temperature influences the 2 m air temperature. During the night, the model overestimates the air temperature in the urban sites, perhaps because the heat load and anthropogenic heat setting (air conditioning switched on for 24 h a day) in the BEM model are larger than the real case, as noted by *Gutiérrez et al.* [2015a]. The model can capture the nighttime UHI phenomenon, although overestimates the UHI magnitude due to the overestimation of the urban air temperature. The usage (including the types and duration) of air conditioning systems needs to be further studied in Hong Kong.

The mean bias error, root-mean-square error (RMSE), and index of agreement (IOA) [*Grimmond et al.*, 2010] for the WRF-BEP-BEM model and observational data from 00:00 UTC (8:00 am local time) in 15 September 2012 to 00:00 UTC in 18 September 2012 are summarized in Table 2. The 2 m air temperature has a mean bias error of 0.07 °C, an RMSE of less than 1.5 °C, and an IOA of 0.93. The statistics show that the WRF-BEP-BEM model can capture the heterogeneity of air temperature. The model overestimates the relative humidity and 10 m wind speed, because, as mentioned above, some stations are located along the coastline and thus are affected by the sea-land breeze circulation.

3.3. Verification With Radiosonde and Wind Profile Data

The observed vertical potential temperature at King's Park (KP, shown in Figure 2c) is used to verify the model simulation. The measurement is taken each day at 00:00 and 12:00 UTC (08:00 A.M. and 08:00 P.M. local time).

Table 2. Verification Statistics for All Available Stations Located in the Innermost Domain of the WRF-BEP-BEM Model From 00:00 UTC on 15 September 2012 to 00:00 UTC on 18 September 2012

Parameter	Number of Stations	Mean Value		Standard Deviation		Mean Bias Error	RMSE	IOA
		Obs.	Sim.	Obs.	Sim.			
2 m air temperature	25	26.29	26.35	2.78	2.55	0.07	1.43	0.93
10 m wind speed	18	2.45	3.15	1.84	1.70	0.70	2.16	0.60
Relative humidity	15	55.70	58.81	11.85	8.19	3.12	10.17	0.72

To better explain the PBL evolution through the day, the vertical potential temperature at 06:00 and 18:00 UTC (2:00 P.M. and 2:00 A.M. local time) is chosen for 16 and 17 September (Figure 7). Due to the height of measurement at KP station, the super adiabatic lapse rate around the ground surface is not presented. However, the model results show a steep near-surface gradient of around 2.5 K and 3 K in the first 100 m layer at 06:00 UTC (2:00 P.M. local time) on both 16 and 17 September.

The model simulation results are verified by using the observed horizontal wind speed and direction obtained from wind profilers at SLW (Figure 2c), near Hong Kong International Airport. The horizontal winds from the ground level up to a height of 1 km are chosen for comparison from 00:00 to 23:00 UTC (08:00 A.M. to 07:00 A.M. local time) on 17 and 18 September (Figure 8). Note that the observations start at 116 m above ground level. The WRF-BEP-BEM model results are generally in good agreement with the observational data. From 04:00 UTC, winds below 500 m turn to the northwest, although the model shows the wind rotation slightly later than the measurement. From 12:00 UTC, winds below 600 m gradually turn to the northeast; the model results show this effect slightly earlier. From 15:00 to 19:00 UTC, the model overestimates the lower level wind speeds by around 1 m/s and fails to capture the stagnation of wind in this period. However, the model captures the wind rotation well, which is important for the study of sea breezes.

4. Effect of Urban Morphology on UHIC and SLBC Development

In section 3, the WRF-BEP-BEM model is shown to be capable of capturing the spatial distribution of air temperature and the diurnal rotation of wind in the innermost domain, at both the surface level and at the height of the lower boundary layer. In this section, three sensitivity tests are carried out to examine the urban effects on the local circulation and boundary layer structure in the Kowloon Peninsula on 17 September 2012.

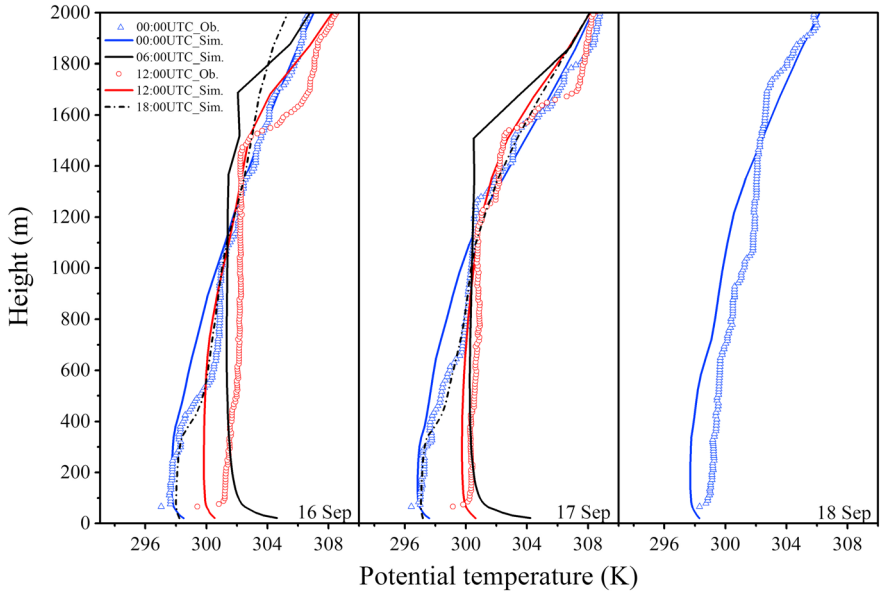

Figure 7. Comparison of observed and simulated vertical profiles of potential temperature (K) at KP Station, as shown in Figure 2c.

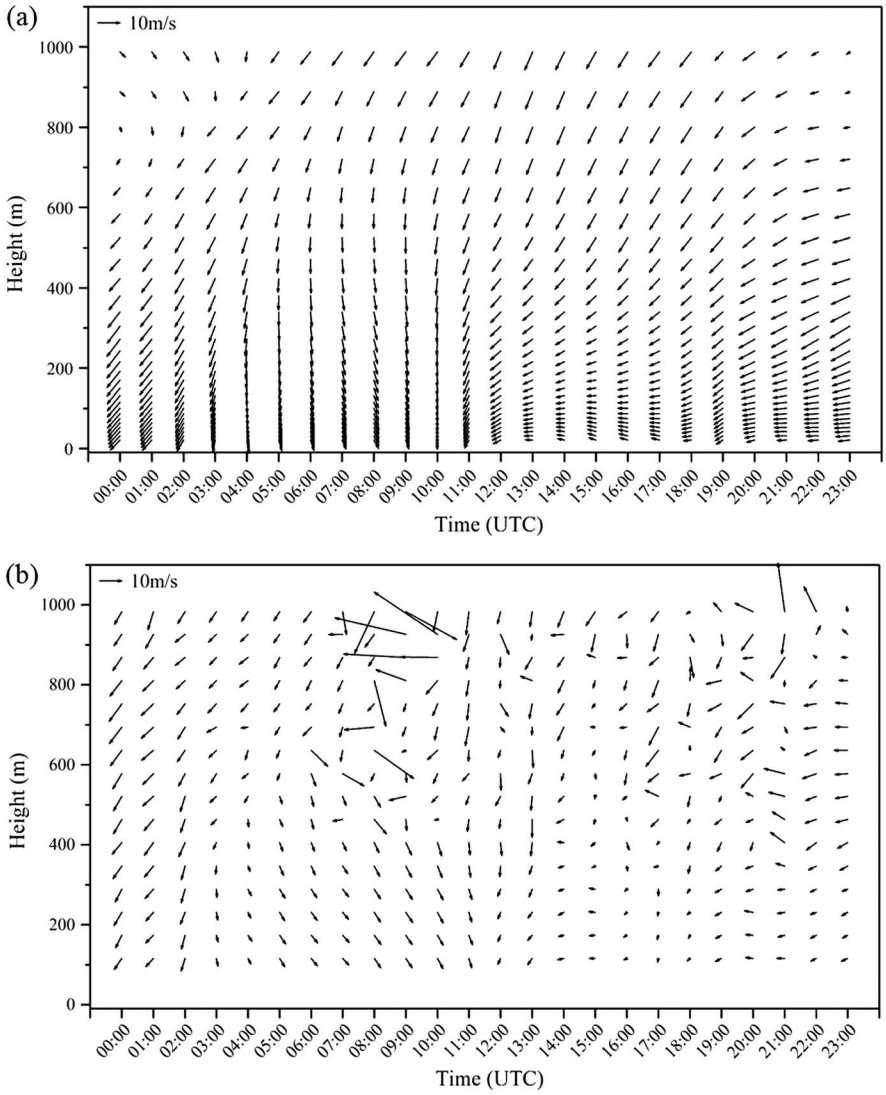

Figure 8. Time-height series of wind speed (m/s) and wind direction for 17 September 2012 at SLW Station near Hong Kong International Airport, as shown in Figure 2c: (a) WRF-BEP-BEM predicted results and (b) wind profiler measurements.

4.1. Influence of Built-Up Areas

To better examine the overall urban heating effect on local circulation and SLBC evolution, the vertical cross sections along transect A–B (Figure 2d) for wind vectors, water vapor ratio, and PBL height are shown in Figure 9. In the Green Case, the urban areas are replaced by grassland, which increases evaporation and evapotranspiration during the day after sunrise and reduces the temperature difference between the land and sea surfaces. At 04:00 UTC (12:00 local time), the WRF-BEP-BEM model shows sea breeze fronts starting to penetrate the Kowloon Peninsula, whereas in the Green Case it penetrates much slower, as shown in Figures 9a1 and 9b1 and 10a2. The 2 m air temperature difference or "urban increment," which largely removes the cloud and topography effects that may alter the surface temperature [*Li et al.*, 2013], reaches around 4.4 °C (Figures 10a1 and 10b1) in the urban areas of the Kowloon Peninsula. The sea breeze front horizontal velocity at a height of 10 m is around 1.5 m/s lower than in the WRF-BEP-BEM model (Figures 10a2 and 10b2). At 08:00 UTC (16:00 local time), the sea breeze fully penetrates urban areas with a much higher vertical velocity but slightly lower PBL height (Figures 9a2 and 9b2) in the WRF-BEP-BEM model than in the Green Case. At this time, the water vapor ratio above ground level shows a dome-shaped profile and propagates much higher (reaching 9.5 g/kg at around 1.4 km in the Baseline Case) than in the Green Case (Figures 9a2 and b2). The UHIC takes in colder air from the urban edge [*Wang and Li*, 2016], which coexists

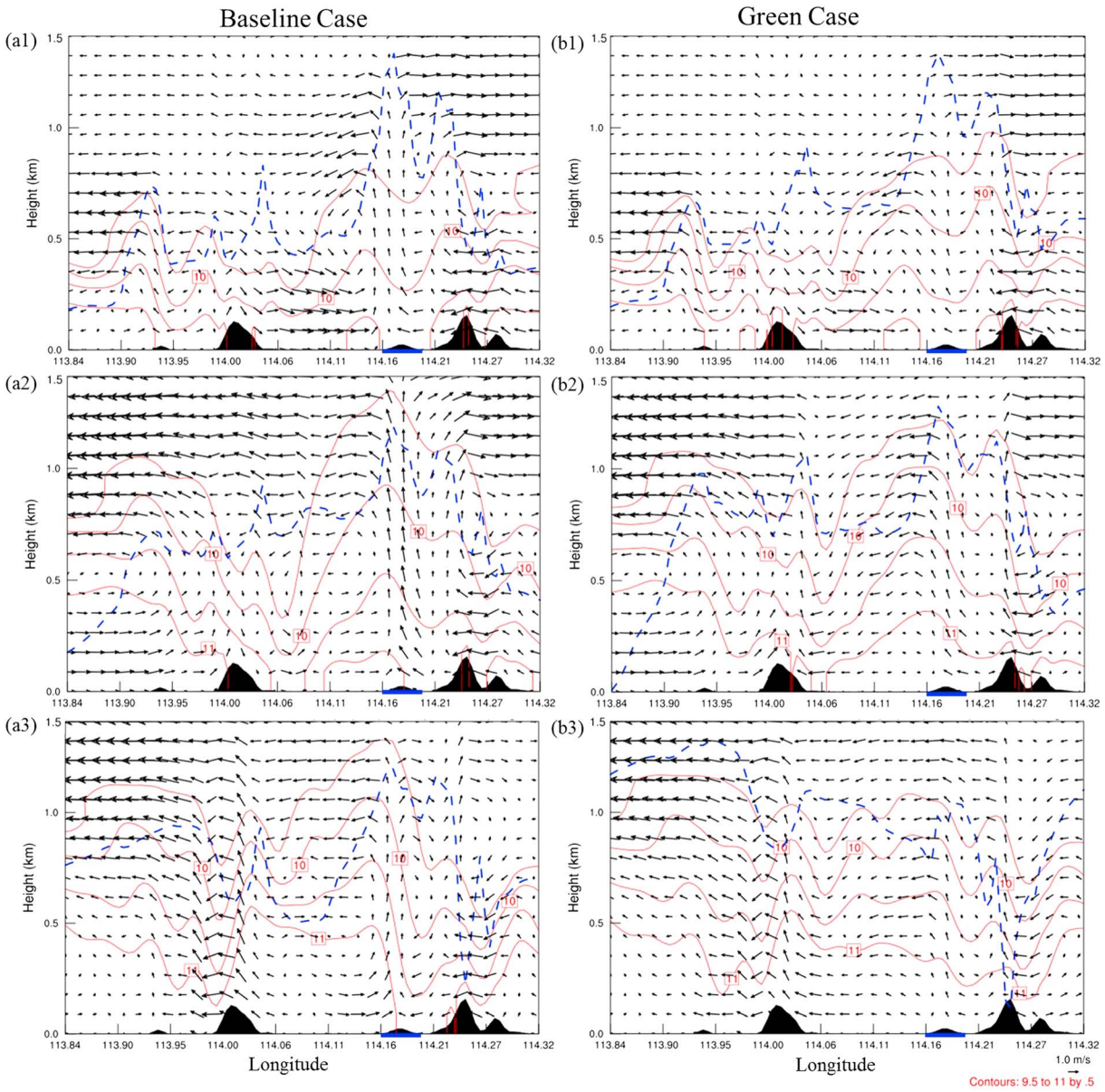

Figure 9. Vertical east-west cross section (transect A–B shown in Figure 2d) of simulated wind vectors (m/s), water vapor ratio (g/kg) (solid red line), and PBL height (km) (dashed blue line) from ground level up to 1.5 km at (a1 and b1) 04:00 UTC, (a2 and b2) , and (a3 and b3) 10:00 UTC (for local time add 8 h) on 17 September 2012. The blue bar at the bottom of the charts indicates the urban region.

with the western sea breeze in the Kowloon Peninsula. The sea breeze inflow due to the UHI could enhance the urban moisture level and enhance upward motion in the convergence zones, which was also reported by *Ryu et al.* [2016] in the Baltimore-Washington metropolitan area. In the Green Case, evaporation and evapotranspiration reduce the moisture level gradient. Whether the UHIC accelerates the circulation of urban moisture is still unclear.

There is a convergence zone in the urban areas (blue bar in Figure 9) with the evolution of a sea breeze, and the PBL height in the convergence zone is much deeper than on both the east and west sides (Figure 9). This limits the mixing effects on the two sides, which inhibits the removal of air pollutants from the surface. This effect is dome-shaped [*Tong et al.*, 2005] and characterized by a high moisture content, high temperature, and high levels of air pollutants. This feature can increase the accumulation of pollutants at the lower PBL height, which has a crucial effect on health. The air quality data at Mong Kok, a roadside station in the urban area in transect A–B, which is monitored by the EPD, show that the concentration of NO_x increased gradually

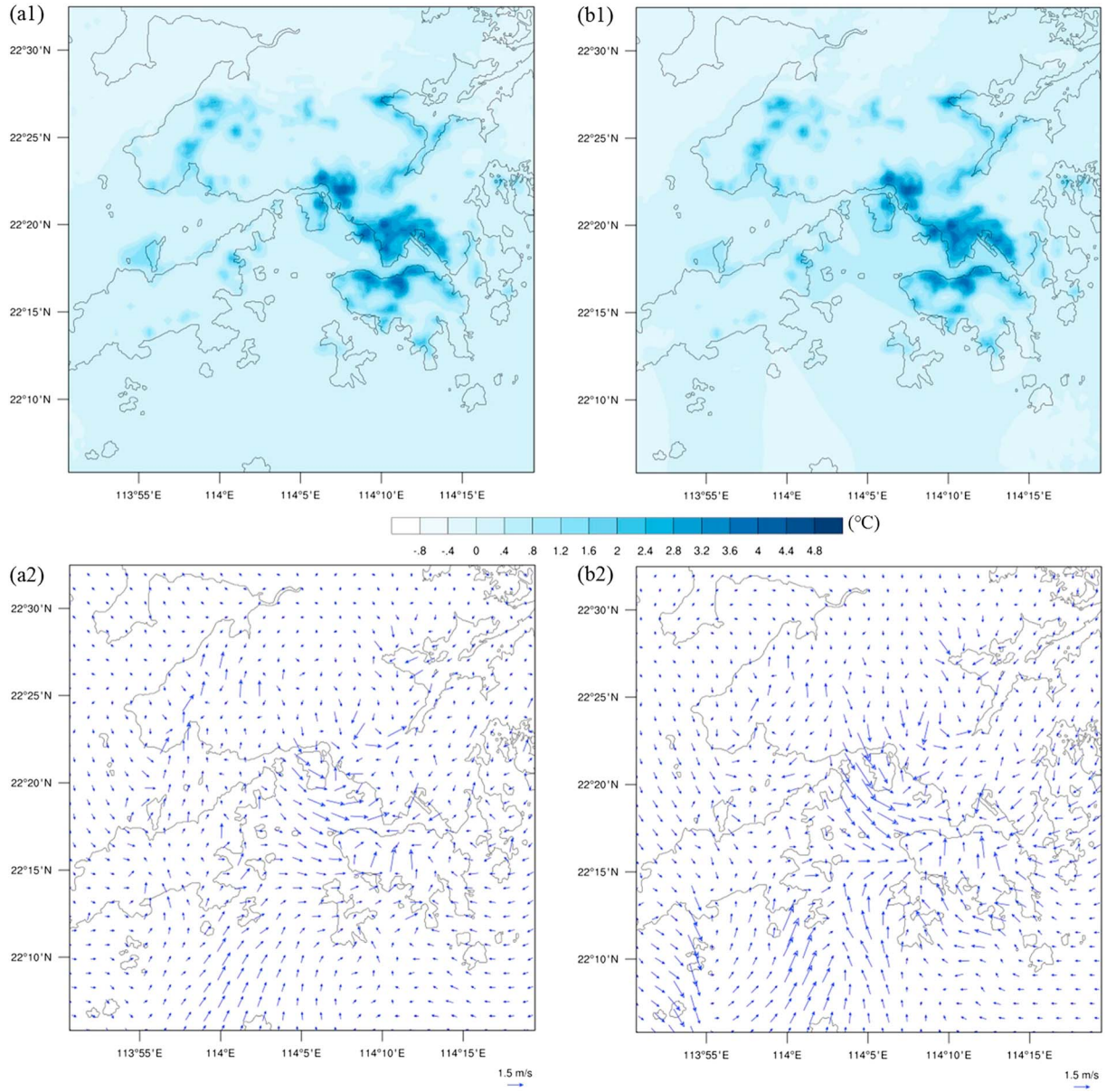

Figure 10. 2 m air temperature difference (°C) (shaded) and 10 m wind difference (Baseline Case-Green Case) at (a1 and a2) 04:00 UTC and (b1 and b2) 06:00 UTC on 17 September 2012.

and reached a peak of 723 μg/m^3 at 11:00 UTC on 17 September. The monitoring results also show that the ozone concentration at Shan Shui Po, which lies in the central part of the Kowloon Peninsula, was over 100 ppb at 06:00 UTC. At 10:00 UTC (18:00 local time), the results from the WRF-BEP-BEM model show weaker sea breezes circulating in the urban areas. In the Green Case, the sea breeze gradually returns to a land breeze, which is consistent with the study by *Chen et al.* [2009] of the onset and offset of sea breezes in the Houston area. In general, the land surface heterogeneity, associated UHIs, and sea-land breeze increase both the strength and duration of low-level convergence.

4.2. Role of Anthropogenic Heat

The BEP and BEM schemes not only consider the effect of buildings on the urban canopy layers but also compute the amount of anthropogenic heat released by air conditioning systems into the atmosphere to maintain the indoor air temperature within a comfortable range [*Salamanca and Martilli*, 2010]. The role of anthropogenic heat on sea breeze development is investigated in a sensitivity test that excludes

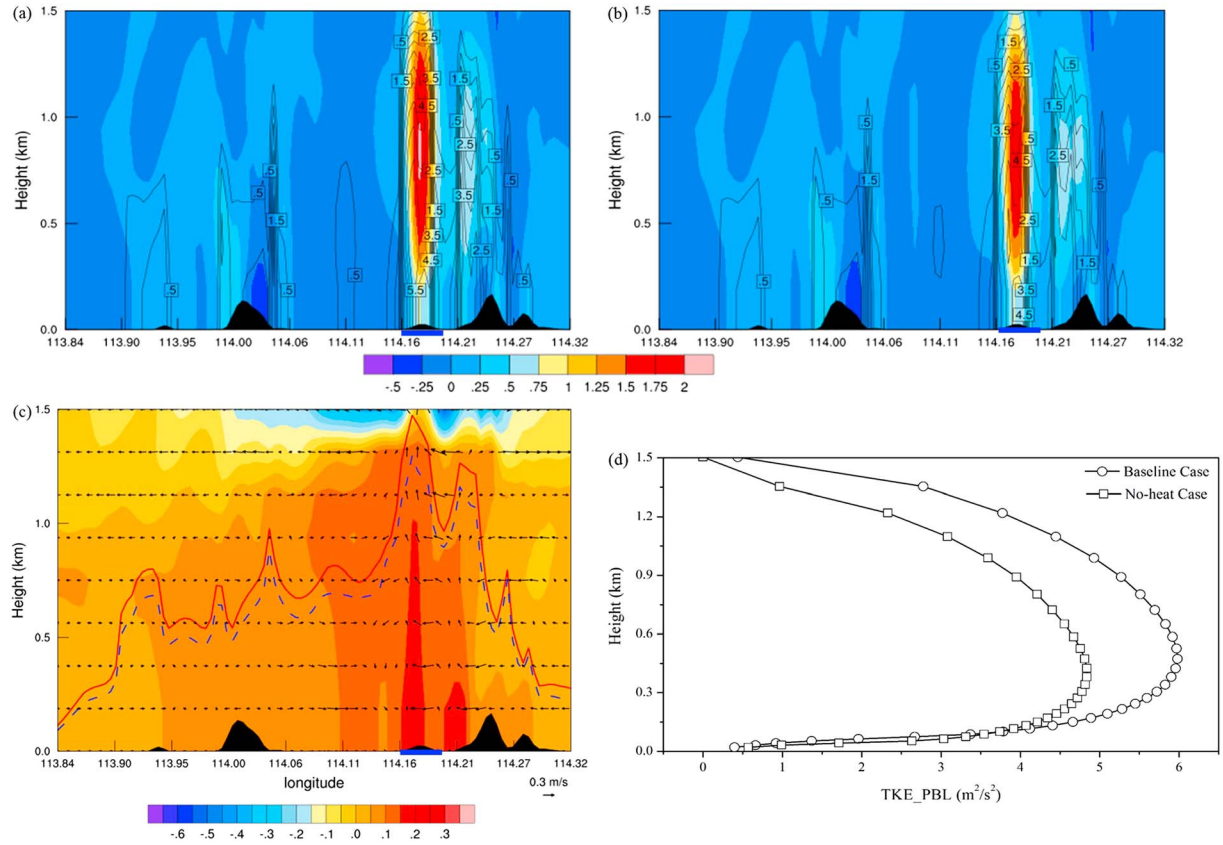

Figure 11. (a) Vertical east-west cross section (transect A–B, shown in Figure 2d) of the WRF-BEP-BEM model simulated vertical velocity (m/s) (shaded) and TKE_PBL (m2/s2) (contour line) above ground level up to 1.5 km at 06:00 UTC (for local time add 8 h) on 17 September 2012. (b) No-heat Case results. (c) Vertical east-west cross section of differences between the two models for wind vector (m/s), temperature (K) (shaded), and PBL height for the WRF-BEP-BEM (dashed blue line) and No-heat Case (solid red line) at 06:00 UTC on 17 September 2012. (d) Vertical profile of TKE_PBL at latitude = 22.32°N, longitude = 114.17°E at 06:00 UTC on 17 September 2012. The blue bar in Figures 11a–11c indicates the urban area.

anthropogenic heat in urban areas. The buildings in the urban grid can absorb solar radiation inside the urban canopy layer and create shear and turbulence due to drag effects [*Oke*, 1988]. The former affects the air temperature indirectly, and the latter can influence vertical mixing in the urban canopy layer. Including anthropogenic heat flux increases the peak value of TKE at around 400 m above ground level (Figures 11a, 11b, and 11d), almost double the height of the No-heat Case, which is around 250 m. The magnitude of TKE is almost double the case without anthropogenic heat. The air pollutants are well mixed at the vertical level at which the maximum TKE value occurs. The release of anthropogenic heat is an important factor for thermal buoyancy flow in the daytime. Within the urban canopy layer, the multilayer schemes introduce a drag force and transform into TKE, which means that the vertical velocity within the urban canopy layer is rather low.

Anthropogenic heat can increase the temperature difference between the land and sea surface, which causes sea breezes to propagate faster on the west side of the Kowloon Peninsula, as shown in Figure 11c. The temperature difference between the surface and around 250 m above the centers of the urban areas, where the convergence zone is formed, is around 0.3°C. A sea breeze front penetrates the land area at 06:00 UTC (14:00 local time); the air temperature decreases by around 0.2 °C due to the advection of cold air from the sea surface (Figure 12a) at the border of the urban areas. The water vapor ratio at 2 m is also slightly higher (not shown here) than in the No-heat Case, due to the sea breeze penetration.

The PBL height is an important factor, and the PBL structure follows the same trend in both numerical experiments. The highest level is around 1.3 km in the urban areas in the WRF-BEP-BEM model, which is slightly lower than in the No-heat Case due to the earlier advection of cold air. When the sea breeze is developing in the WRF-BEP-BEM Case, the PBL height is in the transition from the sea to the land [*Li et al.*, 2013]. A

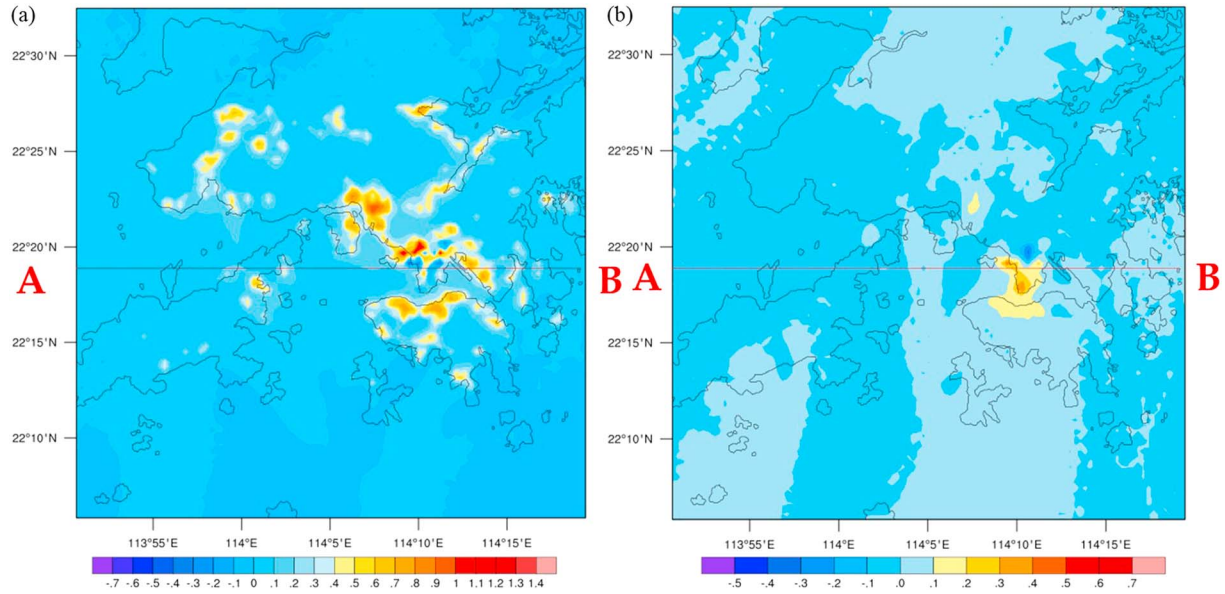

Figure 12. Difference in the 2 m air temperature distribution between the WRF-BEP-BEM and No-heat Case at (a) 06:00 UTC and (b) 21:00 UTC (b) on 17 September 2012. The red line indicates the transect A–B shown in Figure 2d.

dome-shaped feature in the PBL height is captured in the vertical cross section of transect A–B, which is the same shape as that described in section 4.1. Pollutants that are generated inside the urban canopy layers will accumulate and are not easily dispersed from the convergence zone.

We choose 21:00 UTC (05:00 local time), when the 2 m air temperature is at its lowest, to investigate the conditions at night. In the WRF-BEP-BEM model, the 2 m air temperature difference is around 0.1–0.3°C in the urban areas of the Kowloon Peninsula. The diurnal profile of anthropogenic heat flux for the three urban classes in Figure S1 in the supporting information is comparable to the anthropogenic heat values reported in other studies [*Chow et al.*, 2014; *Sailor et al.*, 2015]. The peak anthropogenic heat values are 5, 24, and 55 W/m^2, respectively, for the three urban classes. Note that all three cases assume that air conditioning systems are used for 24 h. The transportation and latent heat flux caused by air conditioning systems are not considered in this study, which may cause some discrepancies in the results.

4.3. Role of Building Drag

In the WRF-BEP-BEM model, a constant drag coefficient was chosen to represent friction and drag forces in the momentum term and TKE production in the urban areas [*Martilli*, 2002]. Although this constant value has been verified in some European cities [*Salamanca et al.*, 2011], using it in a high-density and compact city like Hong Kong overestimates the mean wind speed (Table 2). The sensitivity test in this section implements the new drag coefficient based on the function provided in section 2.2. Table 3 shows the New-drag Case evaluation results for 10 m wind speed, 2 m air temperature, and relative humidity for the stations in Table 2. The implementation of the new BEP-BEM urban parameterization drag coefficient significantly reduces the mean value from 3.15 m/s to 2.63 m/s (also investigated for New York city by *Gutiérrez et al.* [2015b]), and the mean bias error of 10 m wind speed from 0.70 m/s to 0.17 m/s. Meanwhile, the increase in drag force and TKE within the urban canopy layer increases the mean surface air temperature of the 25

Table 3. Verification Statistics for All Available Stations Located in the Innermost Domain for the New-Drag Case From 00:00 UTC on 15 September 2012 to 00:00 UTC on 18 September 2012

Parameter	Number of Stations	Mean Value		Standard Deviation		Mean Bias Error	RMSE	IOA
		Obs.	Sim.	Obs.	Sim.			
2 m air temperature	25	26.29	26.55	2.78	2.72	0.27	1.58	0.91
10 m wind speed	18	2.45	2.63	1.84	1.86	0.17	2.15	0.68
Relative humidity	15	55.70	58.59	11.85	8.46	2.89	11.00	0.68

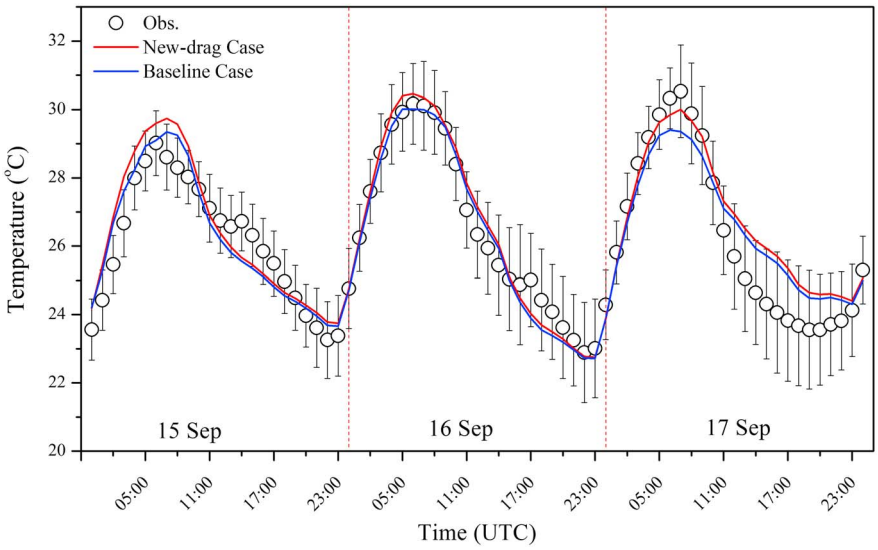

Figure 13. Comparison of observed and predicted 2 m air temperature (°C) for all stations from 00:00 UTC on 15 September 2012 to 00:00 UTC on 18 September 2012 for domain 4 (WRF-BEP-BEM and New-drag Case). The vertical bars represent the standard deviation of 2 m air temperature.

stations by 0.20°C. Figure 13 shows the 2 m temperature profile for the WRF-BEP-BEM and New-drag Case. The latter overestimates the maximum air temperature on 15 and 16 September but better captures the maximum air temperature value on 17 September. Both models overestimate the air temperature during the night of 17 September. Using the new drag coefficient better captures the wind speed within the urban canopy layer (Figure 14), although both models overestimate the wind speed at 12:00 UTC on 17 September. The KP station is inside the convergence zone, where the sea breeze tends to return to a land breeze, and the model does not immediately capture the wind direction, as shown in Figure 13b. However, the New-drag Case explains the wind direction and wind speed within the urban canopy layer better than the Baseline Case.

To better represent the effects of buildings on airflow, the drag force is provided in the momentum equation. However, the constant value of 0.4 in the WRF-BEP-BEM model does not resolve the problem of the large drag force close to the ground, which leads to a large bias in the surface wind speed (Table 2). Changing the drag coefficient according to the gridded λ_P, value significantly increases TKE_PBL inside the urban canopy layer up to 130 m above ground level (26 vertical layers), as shown in Figure 15c. Above the urban canopy layer, TKE_PBL is larger in the WRF-BEP-BEM model due to the different length-scale definitions [*Santiago and Martilli*, 2010, equation 16]. At 06:00 UTC (14:00 local time), the temperature is around 1.3°C higher in the New-drag Case at ground level and around 0.4°C higher at 0.2 km above ground level. Due to turbulence and drag force, the vertical velocity is around 0.1–0.2 m/s less in the urban areas (blue bar in Figures 15a and 15b) and around 0.1–0.2 m/s larger before penetrating inland (longitude = 114.16°) in the New-drag Case (Figures 15a and 15b). The comparison of horizontal velocity in Figure 14 shows that the New-drag Case captures the horizontal velocity better than the WRF-BEP-BEM within the urban canopy layer. When the new drag coefficient is used, the vertical velocity inside the convergence zone ranges from 0 m/s at ground level to around 0.35 m/s at 0.2 km above ground level (not shown here), which can lead to stagnation in urban areas.

The results in Figures 14 and 15 show that using the new drag coefficient, $C_{drag_{new}}$, better represents the horizontal and vertical wind speed within the urban canopy layer, which resolves the problem of overestimation of the surface level wind speed in the baseline case. Moreover, a near-surface temperature inversion below 100 m is found at 00:00 and 12:00 UTC on 17 September 2012 at KP station (shown in Figure S2). An elevated temperature inversion is also found at 00:00 UTC around a height of 350 m. Such temperature inversions could enhance the atmospheric stability near the surface, inhibiting the dispersion of pollutants [*Bei et al.*, 2016]. Figure 16 shows the coexisting effects of SLBC and UHIC. Note that A contains three grid points, a1–a3, which are along the coast, and B contains six grid points, b1–b6, which are inland areas and considered to be in the convergence zone when the sea breeze penetrates. As mentioned above, the sea

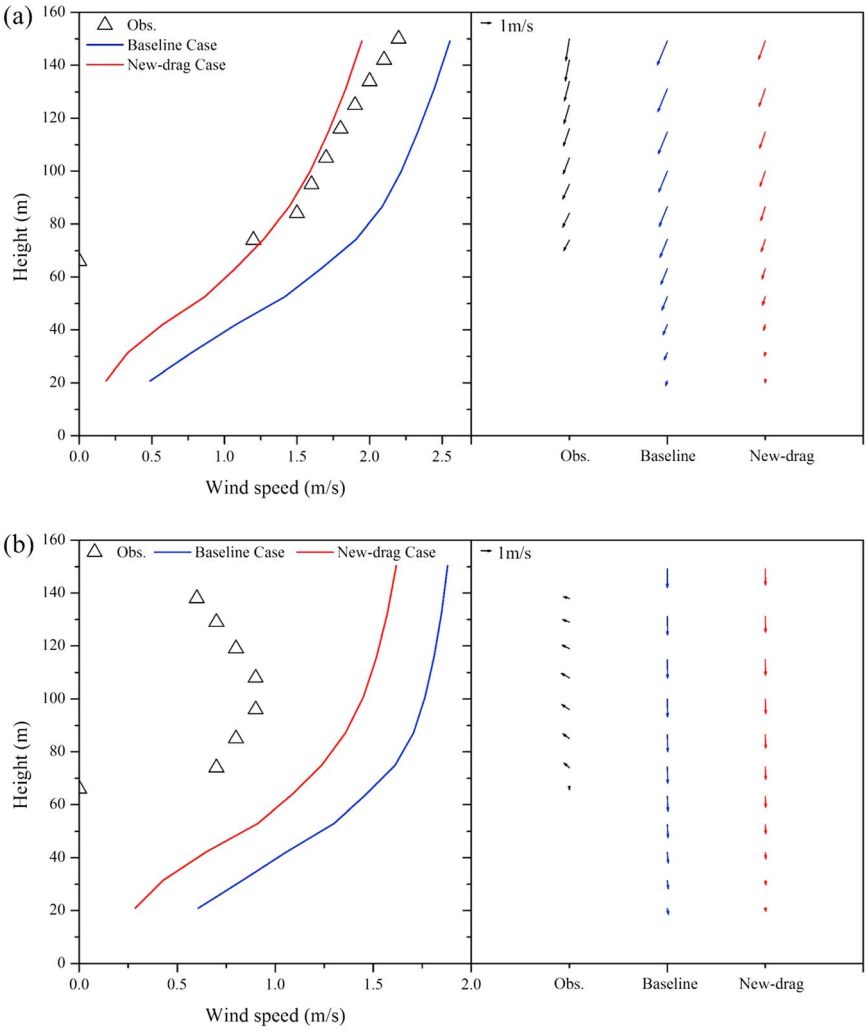

Figure 14. Comparison of horizontal wind speed and wind direction up to 150 m above ground level for observational data, Baseline Case, and New-drag Case at KP station (shown in Figure 2c) at (a) 00:00 UTC and (b) 12:00 UTC on 17 September 2012.

breeze begins to penetrate inland between 03:00 and 04:00 UTC and turns to a land breeze at around 11:00–12:00 UTC, as shown by the dashed red line in Figure 16. For grid points in region A, the horizontal wind speed sharply increases when the sea breeze starts to penetrate inland, and then gradually decreases when it becomes a land breeze. For the grid points in the convergence zone in area B, the horizontal wind speed remains less than 0.5 m/s. The synoptic wind direction is weakly northeasterly when the sea breeze penetrates from the west of the Kowloon Peninsula. The convergence zone forms in the lower level and creates wind stagnation in the urban areas, which inhibits the removal of heat and air pollutants. Although not currently influenced by the sea breeze, the horizontal wind speeds in grids A and B show almost the same trend. The high buildings along the west coast of the Kowloon Peninsula form a "wall" block, as mentioned by *Yim et al.* [2009]. When the synoptic background wind is moderate or weak, UHIC and sea breeze circulation dominate in the urban areas of the Kowloon Peninsula. However, the blocking of the sea breeze penetration contributes to the stagnation of wind and accumulation of local polluting emissions in the lower level convergence zone. Furthermore, the relative humidity measured at KP station at 12:00 UTC (8:00 P.M. local time) on 17 September 2012 is relatively high (55–73%) for up to 1 km, under synoptic conditions of low relative humidity (Figure 3b). Water vapor plays an important role in the heterogeneous reactions for secondary aerosol formation [*Huang et al.*, 2014]. A lower level temperature inversion, low horizontal and vertical wind velocity, and high relative humidity could enhance

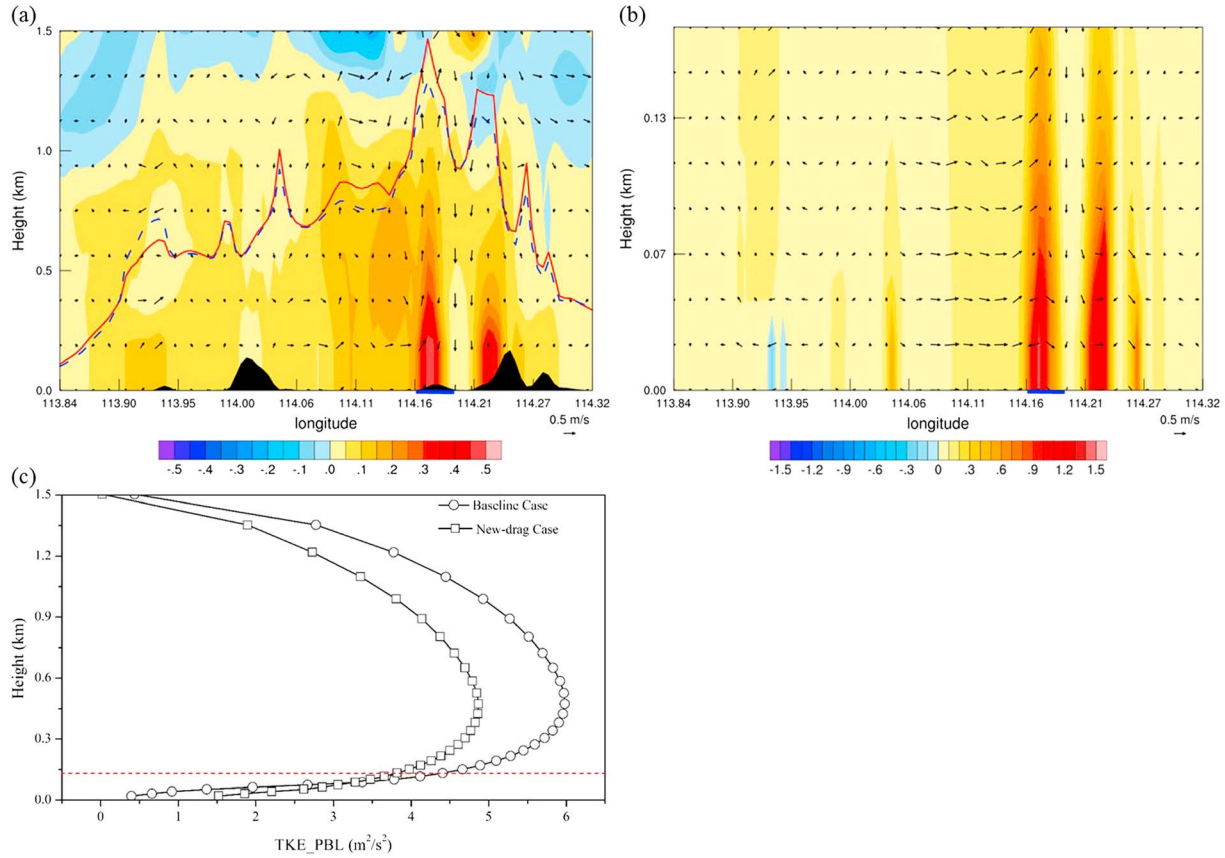

Figure 15. (a) Vertical east-west cross section of wind field (m/s) (vector) and temperature (K) (shaded) differences (New-drag Case-WRF-BEP-BEM Case), and PBL height (WRF-BEP-BEM Case: dashed blue line and New-drag Case: solid red line) up to 1.5 km above ground level at 06:00 UTC on 17 September 2012. (b) Vertical east-west cross section of wind field (m/s) (vector) and temperature (K) (shaded) differences (New-drag Case-Baseline Case) up to 0.2 km above ground level at 06:00 UTC on 17 September 2012. (c) The vertical profile of TKE_PBL at latitude = 22.32°N, longitude = 114.17°E at 06:00 UTC on 17 September 2012. The blue bar in Figures 15a and 15b indicates the urban area.

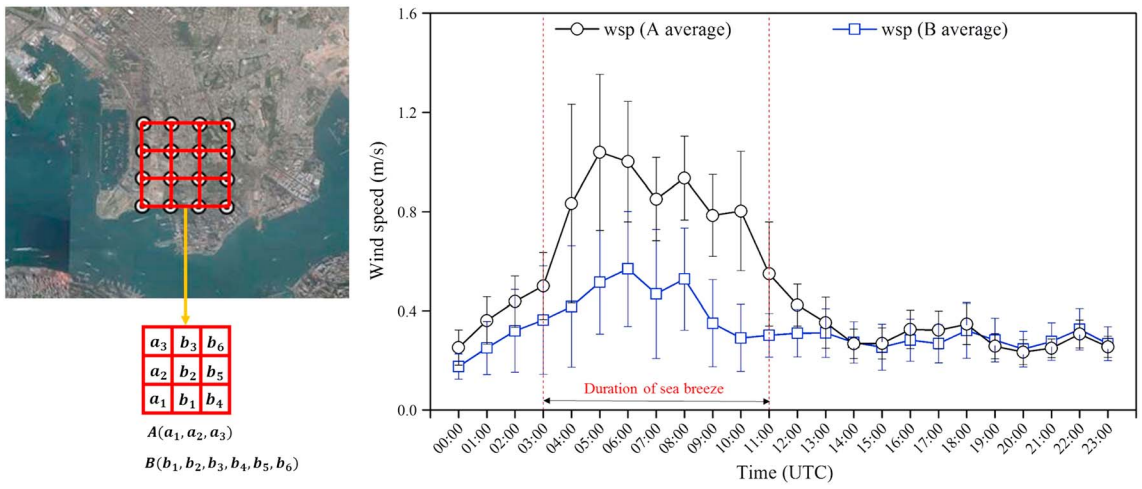

Figure 16. Time series of averaged 10 m horizontal wind speed (m/s) in region A (a1–a3) (black line) and B (b1–b6) (blue line) from 00:00 to 23:00 UTC on 17 September 2012. The vertical bars represent the standard deviation of wind speed.

the accumulation of air pollutants and the formation of secondary aerosols [*Bei et al.*, 2016; *Quan et al.*, 2011]. Therefore, when the northeasterly synoptic wind is weak or moderate, the UHIC and SLBC may contribute to worsening air quality.

5. Conclusions

In this paper, the WRF-BEP-BEM is used to investigate the interactions between sea breezes and urban areas in the high-rise and highly compact city of Hong Kong.

In general, the WRF-BEP-BEM simulation captures the time evolution of the 2 m level temperature distribution reasonably well and overestimates the 10 m wind speed with a mean bias error of 0.70 m/s. A dome-shaped feature, with a high level of moisture and high temperature but less mixing on both the west and east sides of the city, is found when sea breezes develop under weak northeasterly background synoptic wind conditions. The following conclusions can be derived from a series of sensitivity tests.

1. The comparison between the Baseline Case and the Green Case (in which the city is replaced by grass) shows that the city enhances the strong buoyancy motions and takes in more humid air from the land edge.
2. The release of anthropogenic heat affects the development of local circulation. A sensitivity experiment excluding anthropogenic heat in urban areas shows that at 06:00 UTC (2:00 P.M. local time), the sea breeze is fully developed in the urban areas of the Kowloon Peninsula and the temperature difference between the ground level and 250 m varies from around 0.5°C to 0.3°C in the convergence zone area. Anthropogenic heat intensifies the sea breeze circulation and UHIC, which leads to a coastal area surface temperature of around 0.2°C lower than without anthropogenic heat. One possible limitation of this study is that while central air conditioning systems are generally used in commercial buildings in Hong Kong, separate air-cooled air conditioning systems are assumed here for each of the 26 vertical layers. This means that rejected air conditioning heat is released at each vertical layer, whereas the heat release may only occur at certain building floors in large central air conditioning systems. This limitation is expected to be significant on extremely hot days.
3. The study illustrates that a better representation of urban characteristics is needed to study the interaction between the complex morphology and local wind circulations, UHIC, and SLBC, especially in the coastal area. A new drag coefficient based on the plan area per unit ground area, λ_P, is implemented for the Kowloon Peninsula. Besides the basic characteristics captured by the baseline model, the new coefficient captures the lower level temperature inversion, low horizontal and vertical wind velocity, and high relative humidity. Moreover, the New-drag Case captures the stagnation in the lower level convergence zone, which is even more important than improving the description of the air temperature distribution in a high-rise and high compact city, because the wind stagnation in low-level convergence zones is a critical factor for air pollution problems.

Acknowledgments
This work received financial support from the Hong Kong SAR government: RGC CRF project HKU9/CRF/12G. The weather data for individual stations were obtained through collaboration with the Hong Kong Observatory. The authors thank the Hong Kong Planning Department and Hong Kong Lands Department for the land use and land cover, building GIS, and MODIS data. The input and output data used in this study are available upon request from the corresponding author at liyg@hku.hk for academic research purposes. M.S. Wong was supported in part by a General Research Fund (project ID: 15205515) from the Research Grants Council of Hong Kong.

References

Arnfield, A. J. (2003), Two decades of urban climate research: A review of turbulence, exchanges of energy and water, and the urban heat island, *Int. J. Climatol.*, *23*, 1–26, doi:10.1002/joc.859.

Bei, N., B. Xiao, N. Meng, and T. Feng (2016), Critical role of meteorological conditions in a persistent haze episode in the Guanzhong basin, China, *Sci. Total Environ.*, *550*, 273–284, doi:10.1016/j.scitotenv.2015.12.159.

Bougeault, P., and P. Lacarrere (1989), Parameterization of orography-induced turbulence in a mesobeta-scale model, *Mon. Weather Rev.*, *117*(8), 1872–1890.

Burian, S., N. Augustus, I. Jeyachandran, and M. Brown (2007), National building statistics database: Version 2, LA-UR-08-1921.

Castles, S., H. De Haas, and M. J. Miller (2013), Migration, security and the debate on climate change, in *The Age of Migration: International Population Movements in the Modern World*, edited by P. Macmillan, pp. 198–213, New York.

Chan, L. Y., C. Y. Chan, and Y. Qin (1998), Surface ozone pattern in Hong Kong, *J. Appl. Meteorol. Climatol.*, *37*(10), 1151–1165.

Chan, C. Y., and L. Y. Chan (2000), Effect of meteorology and air pollutant transport on ozone episodes at a subtropical coastal Asian city, Hong Kong, *J. Geophys. Res.*, *105*(16), 20,707–20,724.

Chen, F., and J. Dudhia (2001), Coupling an advanced land surface-hydrology model with the Penn State-NCAR MM5 modeling system. Part I: Model implementation and sensitivity, *Mon. Weather Rev.*, *129*(4), 569–585.

Chen, F., S. Miao, M. Tewari, J. W. Bao, and H. Kusaka (2009), A numerical study of interactions between surface forcing and sea breeze circulations and their effects on stagnation in the greater Houston area, *J. Geophys. Res.*, *116*, D12105, doi:10.1029/2010JD015533.

Chen, F., X. Yang, and W. Zhu (2014), WRF simulations of urban heat island under hot-weather synoptic conditions: The case study of Hangzhou City, China, *Atmos. Res.*, *138*, 364–377.

Chow, W. T., F. Salamanca, M. Georgescu, A. Mahalov, J. M. Milne, and B. L. Ruddell (2014), A multi-method and multi-scale approach for estimating city-wide anthropogenic heat fluxes, *Atmos. Environ.*, *99*, 64–76.

Coceal, O., and S. E. Belcher (2005), Mean winds through an inhomogeneous urban canopy, *Boundary Layer Meteorol.*, *115*(1), 47–68, doi:10.1007/s10546-004-1591-4.

Di Sabatino, S., L. S. Leo, R. Cataldo, C. Ratti, and R. Britter (2010), Construction of digital elevation models for a southern European city and a comparative morphological analysis with respect to northern European and North American cities, *J. Appl. Meteorol. Climatol.*, *49*(7), 1377–1396, doi:10.1175/2010JAMC2117.1.

Dudhia, J. (1989), Numerical study of convection observed during the Winter Monsoon Experiment using a mesoscale two-dimensional model, *J. Atmos. Sci.*, *46*, 3077–3107.

Grimmond, C. S. B., and T. R. Oke (1999), Heat storage in urban areas: Local-scale observations and evaluation of a simple model, *J. Appl. Meteorol.*, *38*, 922–940.

Grimmond, C. S. B., et al. (2010), The international urban energy balance models comparison project: First results from phase 1, *J. Appl. Meteorol. Climatol.*, *49*(6), 1268–1292, doi:10.1175/2010JAMC2354.1.

Gutiérrez, E., J. E. González, A. Martiili, R. Bornstein, and M. Arend (2015a), Simulations of a heat-wave event in New York City using a multilayer urban parameterization, *J. Appl. Meteorol. Climatol.*, *54*(2), 283–302, doi:10.1175/JAMC-D-14-0028.1.

Gutiérrez, E., A. Martiili, J. L. Santiago, and J. E. González (2015b), A mechanical drag coefficient formulation and urban canopy parameter assimilation technique for complex urban environments, *Boundary Layer Meteorol.*, *157*, 333–341, doi:10.1007/s10546-015-0051-7.

Holt, T., and J. Pullen (2007), Urban canopy modeling of the New York City metropolitan area: A comparison and validation of single and multilayer parameterizations, *Mon. Weather Rev.*, *135*, 1906–1930.

Hong, S., J. Dudhia, and S. Chen (2004), A revised approach to ice microphysical processes for the bulk parameterization of clouds and precipitation, *Mon. Weather Rev.*, *132*(1), 103–120.

Huang, R. J., et al. (2014), High secondary aerosol contribution to particulate pollution during haze events in China, *Nature*, *514*(7521), 218–222, doi:10.1038/nature13774.

Hunt, J. C., Y. V. Timoshkina, S. I. Bohnenstengel, and S. Belcher (2013), Implications of climate change for expanding cities worldwide, *Proceedings of the ICE - Urban Design and Planning*, *166*(4), 241–254.

Johnson, G. T., T. R. Oke, T. J. Lyons, D. G. Steyn, I. D. Watson, and J. A. Voogt (1991), Simulation of surface urban heat islands under 'ideal' conditions at night, part I: Theory and tests against field data, *Boundary Layer Meteorol.*, *56*, 275–294.

Kain, J., and J. Fritsch (1990), A one-dimensional entraining/detraining plume model and its application in convective parameterization, *J. Atmos. Sci.*, *47*, 2784–2802.

Kondo, H., Y. Genchi, Y. Kikegawa, Y. Ohashi, H. Yoshikado, and H. Komiyama (2005), Development of a multi-layer urban canopy model for the analysis of energy consumption in a big city: Structure of the urban canopy model and its basic performance, *Boundary Layer Meteorol.*, *116*(3), 395–421, doi:10.1007/s10546-005-0905-5.

Kusaka, H., H. Kondo, Y. Kikegawa, and F. Kimura (2001), A simple single-layer urban canopy model for atmospheric models: Comparison with multi-layer and slab models, *Boundary Layer Meteorol.*, *101*(3), 329–358.

Li, X.-X., T.-Y. Koh, D. Entekhabi, M. Roth, J. Panda, and L. K. Norford (2013), A multi-resolution ensemble study of a tropical urban environment and its interactions with the background regional atmosphere, *J. Geophys. Res. Atmos.*, *118*, 9804–9818, doi:10.1002/jgrd.50795.

Li, X.-X., T. Y. Koh, J. Panda, and L. K. Norford (2016), Impact of urbanization patterns on the local climate of a tropical city Singapore: An ensemble study, *J. Geophys. Res. Atmos.*, *121*, 4386–4403, doi:10.1002/2015JD024452.

Liu, Y., F. Chen, T. Warner, and J. Basara (2006), Verification of a meso-scale data assimilation and forecasting system for the Oklahoma City area during the Joint Urban 2003 Field Project, *J. Appl. Meteorol. Climatol.*, *45*(7), 912–929.

Lo, J. C. F., A. K. H. Lau, F. Chen, J. C. H. Fung, and K. K. M. Leung (2006), Urban modification in a mesoscale model and the effects on the local circulation in the Pearl River Delta region, *J. Appl. Meteorol. Climatol.*, *46*, 457–476, doi:10.1175/JAM2477.1.

Martilli, A. (2002), Numerical study of urban impact on boundary layer structure: Sensitivity to wind speed, urban morphology, and rural soil moisture, *J. Appl. Meteorol.*, *41*(12), 1247–1266.

Martilli, A., A. Clappier, and M. W. Rotach (2002), An urban surface exchange parameterization for mesoscale models, *Boundary Layer Meteorol.*, *104*, 261–304, doi:10.1023/A:1016099921195.

Martilli, A., Y. A. Roulet, M. Junier, F. Kirchner, M. W. Rotach, and A. Clappier (2003), On the impact of urban surface exchange parameterizations on air quality simulations: The Athens case, *Atmos. Environ.*, *37*, 4217–4231.

Masson, V. (2000), A physically-based scheme for the urban energy budget in atmospheric models, *Boundary Layer Meteorol.*, *94*(3), 357–397.

Miao, S., F. Chen, M. A. LeMone, M. Tewari, Q. Li, and Y. Wang (2009), An observational and modeling study of characteristics of urban heat island and boundary layer structures in Beijing, *J. Appl. Meteorol. Climatol.*, *48*(3), 484–501, doi:10.1175/2008JAMC1909.1.

Mlawer, E., S. Taubman, P. Brown, M. Iacono, and S. Clough (1997), Radiative transfer for inhomogeneous atmosphere: RRTM, a validated correlated-k model for longwave, *J. Geophys. Res.*, *102*, 16663–16682.

Oke, T. R. (1988), Street design and urban canopy layer climate, *Energy Build.*, *11*(1), 103–113.

Oleson, K. W., G. B. Bonan, J. Feddema, M. Vertenstein, and C. S. B. Grimmond (2008), An urban parameterization for a global climate model. Part I: Formulation and evaluation for two cities, *J. Appl. Meteorol. Climatol.*, *47*(4), 1038–1060, doi:10.1175/2007JAMC1597.1.

Quan, J., Q. Zhang, H. He, J. Liu, M. Huang, and H. Jin (2011), Analysis of the formation of fog and haze in north China plain (NCP), *Atmos. Chem. Phys.*, *11*(15), 8205–8214, doi:10.5194/acp-11-8205-2011.

Raupach, M. R. (1992), Drag and drag partition on rough surfaces, *Boundary Layer Meteorol.*, *60*, 375–395.

Rizwan, A. M., L. Y. C. Dennis, and C. Liu (2008), A review on the generation, determination and mitigation of urban heat island, *J. Environ. Sci.*, *20*, 120–128, doi:10.1016/S1001-0742(08)60019-4.

Ryu, Y. H., J. A. Smith, E. Bou-Zeid, and M. L. Baeck (2016), The influence of land surface heterogeneities on heavy convective rainfall in the Baltimore-Washington metropolitan area, *Mon. Weather Rev.*, *144*(2), 553–573, doi:10.1175/MWR-D-15-0192.1.

Sailor, D. J., M. Georgescu, J. M. Milne, and M. A. Hart (2015), Development of a national anthropogenic heating database with an extrapolation for international cities, *Atmos. Environ.*, *118*, 7–18.

Salamanca, F., and A. Martilli (2010), A new building energy model coupled with an urban canopy parameterization for urban climate simulations. Part I. Formulation, verification and a sensitive analysis of the model, *Theor. Appl. Climatol.*, *99*, 331–344, doi:10.1007/s00704-009-0142-9.

Salamanca, F., A. Martilli, M. Tewari, and F. Chen (2011), A study of the urban boundary layer using different urban parameterizations and high-resolution urban canopy parameters with WRF, *J. Appl. Meteorol. Climatol.*, *50*(5), 1107–1128, doi:10.1175/2010JAMC2538.1.

Salamanca, F., A. Martilli, and C. Yague (2012), A numerical study of the urban heat island over Madrid during the DESIREX (2008) campaign with WRF and evaluation of simple mitigation strategies, *Int. J. Climatol.*, *32*(15), 2372–2386, doi:10.1002/joc.3398.

Salamanca, F., M. Georgescu, A. Mahalov, M. Moustaoui, and M. Wang (2014), Anthropogenic heating of the urban environment due to air conditioning, *J. Geophys. Res. Atmos.*, *119*, 1–17, doi:10.1002/2013JD021225.

Santiago, J. L., O. Coceal, A. Martilli, and S. E. Belcher (2008), Variation of the sectional drag coefficient of a group of buildings with packing density, *Boundary Layer Meteorol.*, *128*(3), 445–457, doi:10.1007/s10546-008-9294-x.

Santiago, J. L., and A. Martilli (2010), A dynamic urban canopy parameterization for mesoscale models based on computational fluid dynamics Reynolds-averaged Navier-Stokes microscale simulations, *Boundary Layer Meteorol.*, *137*(3), 417–439, doi:10.1007/s10546-010-9538-4.

Siu, L. W., and M. A. Hart (2013), Quantifying urban heat island intensity in Hong Kong SAR, China, *Environ. Monit. Assess.*, *185*(5), 4383–4398.

Skamarock, W. C., J. B. Klemp, J. Dudhia, D. O. Gill, D. Barke, M. G. Duda, X. Y. Huang, and W. Wang (2008), A description of the Advanced Research WRF version 3 (NCAR/TN-475+STR), NCAR Technical Note, doi:10.5065/D68S4MVH.

Silva, H. R., R. Bhardwaj, P. E. Phelan, J. S. Golden, and S. Grossman-Clarke (2009), Development of a zero-dimensional mesoscale thermal model for urban climate, *J. Appl. Meteorol. Climatol.*, *48*(3), 657–668, doi:10.1175/2008JAMC1962.1.

Tong, H., A. Walton, J. Sang, and J. C. L. Chan (2005), Numerical simulation of the urban boundary layer over the complex terrain of Hong Kong, *Atmos. Environ.*, *39*(19), 3549–3563.

Uno, I., H. Ueda, and S. Wakamatsu (1989), Numerical modelling of the nocturnal urban boundary layer, *Boundary Layer Meteorol.*, *49*(1), 77–98, doi:10.1007/BF00116406.

Wang, X., and Y. Li (2016), Predicting urban heat island circulation using CFD, *Build. Environ.*, *99*, 82–97.

Wang, Z. H., E. Bou-Zeid, and J. A. Smith (2013), A coupled energy transport and hydrological model for urban canopies evaluated using a wireless sensor network, *Q. J. R. Meteorol. Soc.*, *139*, 1643–1657, doi:10.1002/qj.2032.

Wu, J.-B., K. C. Chow, J. C. H. Fung, A. K. H. Lau, and T. Yao (2011), Urban heat island effects of the Pearl River Delta city clusters—Their interactions and seasonal variation, *Theor. Appl. Climatol.*, *103*, 489–499, doi:10.1007/s00704-010-0323-6.

Yang, X., Y. Li, Z. Luo, and P. W. Chan (2016), The urban cool island phenomenon in a high-rise high-density city and its mechanisms, *Int. J. Climatol.*, doi:10.1002/joc.4747.

Yim, S. H. L., J. C. H. Fung, A. K. H. Lau, and S. C. Kot (2009), Air ventilation impacts of the "wall effect" resulting from the alignment of high-rise buildings, *Atmos. Environ.*, *43*(32), 4982–4994.

Zhang, L., and M. Zhang (1997), Study of the sea-land breeze system in Hong Kong, *HKMetS Bulletin*, *7*(1), 22–42.